The Impact and Mechanism of the Magnetic Inclination Angle on O+ Escape from Mars

Shibang Li, Haoyu Lu, Jinbin Cao, Christian Mazelle, Jun Cui, Zhaojin Rong, James A Wild, Yiqun Yu, Xing Li, Yun Li, et al.

The Astrophysical Journal, 931:30 (7pp), 2022 May 20 https://doi.org/10.3847/1538-4357/ac6510

The Impact and Mechanism of the Magnetic Inclination Angle on O^+ Escape from Mars

Shibang Li[1], Haoyu Lu[1,2,8], Jinbin Cao[1,2], Christian Mazelle[3], Jun Cui[4], Zhaojin Rong[5,6], James A. Wild[7], Yiqun Yu[1,2], Xing Li[1,2], Yun Li[1], and Guokan Li[1]
[1] School of Space and Environment, Beihang University, Beijing, 100191, People's Republic of China; lvhy@buaa.edu.cn
[2] Key Laboratory of Space Environment Monitoring and Information Processing, Ministry of Industry and Information Technology, Beijing, 100191, People's Republic of China
[3] Institute de Recherche en Astrophysique et Planetologie, CNRS—University of Toulouse—CNES, Toulouse, France
[4] School of Atmospheric Sciences, Sun Yat-Sen University, Zhuhai, People's Republic of China
[5] Institute of Geology and Geophysics, Chinese Academy of Sciences, Beijing, People's Republic of China
[6] College of Earth and Planetary Sciences, University of Chinese Academy of Sciences, Beijing, People's Republic of China
[7] Department of Physics, Lancaster University, Lancaster, UK
Received 2021 October 29; revised 2022 April 4; accepted 2022 April 5; published 2022 May 20

Abstract

Ion escape from the atmosphere to space is one of the most likely reasons to account for the evolution of the Martian climate. Based on three-dimensional multifluid magnetohydrodynamic simulations, we investigated the impact of the magnetic inclination angle on O^+ escape at low altitudes of 275–1000 km under the typical solar wind conditions. Numerical results showed that an outward ion velocity in the direction opposite to the electromagnetic (EM) force results in weak outward flux and leads to ions becoming trapped by the horizontal magnetic field lines at the local horizontal magnetic equator. Much of the EM force can be attributed to the Hall electric force. In the region of high absolute magnetic inclination angle, the outward ion velocity has the same direction as the EM force, which increases the outward flux and causes ions to diffuse upward along open magnetic field lines to higher altitude. In addition, the EM force is mainly provided by the electron pressure gradient force and the motional electric force. Global results for the magnetic inclination angle indicate that the strong crustal field regions in the southern hemisphere are mainly occupied by magnetic field lines with high absolute magnetic inclination angle, while horizontal field lines are dominant in the northern hemisphere, which leads to a higher O^+ escape rate in the Martian southern hemisphere than in the northern, from altitudes of 275 to 1000 km. This is a significant advance in understanding the impact and mechanism of the Martian magnetic field directions on ion escape.

Unified Astronomy Thesaurus concepts: Mars (1007); Solar-planetary interactions (1472); Magnetic anomalies (993); Magnetohydrodynamics (1964)

1. Introduction

Mars is the most Earthlike planet in the solar system and one of the most accessible extraterrestrial bodies for interplanetary probes, which has made it a hotspot for planetary science research in recent decades. It is believed that the current status of Mars has important implications for understanding the evolutionary history of Earth's atmosphere (e.g., Seager 2013; Airapetian et al. 2017; Dong et al. 2017, 2018). Studies have shown that ancient Mars may have had a thicker atmosphere and abundant water resources with a warm and wet climate (e.g., Carr 1986, 2007; Jakosky & Phillips 2001), but the long-term escape of atmospheric water made Mars gradually evolve into the dry and cold planet of the present day (Lillis et al. 2015; Jakosky & Russell 2015; Jakosky et al. 2017, 2018). Therefore, atmospheric ion escape has become one of the core scientific subjects of several Mars exploration missions, such as Mars Express in Europe (Chicarro et al. 2004), Mars Atmosphere and Volatile Evolution (MAVEN) in the United States (Jakosky et al. 2015), and the recent Tianwen-1 in China (Wan et al. 2020).

Mars has a dense upper atmosphere composed mainly of CO_2 and O, together with CO and N_2 (Mahaffy et al. 2015). The neutral components are ionized by solar radiation, charge exchange with solar wind protons, and the impact of energetic electrons to form the ionosphere (e.g., Nagy et al. 2004; Bougher et al. 2015). The nightside ionosphere is formed by either solar wind electron precipitation or day-to-night plasma transport (Xu et al. 2016; Cui et al. 2019). Due to the absence of a strong global magnetic field on Mars, the solar wind can interact closely with the Martian ionosphere, transferring energy and momentum effectively. Moreover, regions with magnetized crust appear as magnetic anomalies concentrated in the southern hemisphere of the Martian surface (Acuña et al. 2001). The strongest of these crustal magnetic fields is nearly 650 nT at 200 km altitude over latitudes of 53°S and longitudes between 120°W and 210°W (Langlais et al. 2004), but locally it can reach 1500 nT at 100 km above Terra Sirenum and Terra Cimmeria in the southern highlands around longitude 180°E (Connerney et al. 1999).

Previous studies of ion escape mechanisms have revealed that there are several processes through which the ions can escape to space, including ion pickup (Dong et al. 2015a), ion sputtering (Johnson & Leblanc 2001), charge exchanges (Shizgal & Arkos 1996), and ionospheric outflow (Fränz et al. 2015). Moreover, ion kinetic processes can play a significant role in ion escape. For example, the pickup process (the ion plume) is due to ions picked by the convection electric field ($E_{SW} = -U_{SW} \times B_{SW}$) and therefore ions are subject to a

[8] Corresponding author.

force $F_{SW} = qE_{SW}$, where U_{SW} is the solar wind velocity and B_{SW} is the interplanetary magnetic field (IMF). The $J \times B$ force due to the magnetic shear stresses of the draped magnetic field lines becomes strongest in the Martian plasma sheet, where ions can gain additional acceleration from this force (Halekas et al. 2006; Dubinin et al. 2017a). Ionospheric outflow, also named polar wind, refers to the outflow of ions accelerated by ambipolar electric fields ($-\nabla p_e$) along open magnetic field lines that are stretched in the tailward direction (Collinson et al. 2015). The escape of ions through these processes, as well as ion escape trajectories, can be critically influenced by the plasma environment produced by the interaction between the planet and the solar wind.

It is well known that the Martian crustal field affects both ion escape processes and ion escape rates from numerous investigations by means of observational analysis and model simulation. However, there is still a controversy over whether the planetary magnetic field prohibits atmospheric erosion or, on the contrary, enhances ion loss. Some researchers have suggested that the crustal field protects the Martian atmosphere from erosion, which is more efficient when the strong crustal fields are located at subsolar longitudes. Ramstad et al. (2016) revealed that variations in the dayside orientation of crustal field due to Martian rotation modulate the ion escape rate with a minimum escape rate for low solar zenith angle (28°–60°). Numerical simulations showed that the crustal magnetic field has a shielding effect that protects the Martian atmosphere, with the strongest effect under perihelion conditions when the main crustal field is located on the subsolar area (Ma et al. 2014; Dong et al. 2015b). Recently, Fan et al. (2019) revealed the protective effect of the Martian crustal field on dayside ions and the reduction of outward fluxes.

Some researchers have suggested that the crustal field plays a role in enhancing the ion loss. Early studies indicated that the crustal anomalies enhance escape by forming flux ropes along elongated crustal field lines (Brain et al. 2010; Harnett 2009). The numerical simulation presented by Sakai et al. (2018) suggested that when a weak intrinsic dipole magnetic field is present on Mars, the ion escape rate increases. Moreover, numerous studies have suggested that the impact of crustal field on the ion escape rate depends on the orientation and strength of magnetic field formed in an inflated ionosphere over vertical field regions, resulting in an increase in ion escape rate (Matta et al. 2015; Egan et al. 2019; Wu et al. 2019).

However, the physical mechanisms causing the suppression or enhancement effects of the Martian magnetic field on the escape of ions are still open questions. In this study, we investigate the mechanisms by which the Martian magnetic inclination angle influences O^+ escape using a three-dimensional multifluid magnetohydrodynamic (MHD) numerical model, which is useful for understanding how the magnetic field direction affects the escape of Martian atmospheric ions from both local and global perspectives.

2. Model Description

The 3D multifluid MHD simulation model used in this paper solves separate mass, momentum, and energy equations for the four ion species, i.e., H^+, O_2^+, O^+, CO_2^+, which are the main ionospheric components detected by MAVEN (Benna et al. 2015). The governing fluid equations for each species can be expressed as follows (Najib et al. 2011):

$$\frac{\partial \rho_s}{\partial t} + \nabla \cdot (\rho_s u_s) = \frac{\delta \rho_s}{\delta t} \tag{1a}$$

$$\frac{\partial (\rho_s u_s)}{\partial t} + \nabla \cdot (\rho_s u_s u_s + I p_s) = n_s q_s (u_s - u_+) \times B + \frac{n_s q_s}{n_e e}(J \times B - \nabla p_e) + \frac{\delta M_s}{\delta t} \tag{1b}$$

$$\frac{\partial e_s}{\partial t} + \nabla \cdot [(e_s + p_s) u_s] = u_s \cdot \left[\frac{n_s q_s}{n_e e}(J \times B - \nabla p_e) + n_s q_s (u_s - u_+) \times B \right] + \frac{\delta E_s}{\delta t} \tag{1c}$$

where $e_s = \frac{1}{2}\rho_s u_s^2 + \frac{p_s}{\gamma - 1}$. Here ρ_s, u_s, p_s, n_s, and q_s are the individual mass density, velocity, pressure of the ions, number density, and charge respectively. B is the magnetic field and I is the identity matrix. p_e and n_e are the pressure and number density of electrons; γ is the polytropic index, chosen to be $5/3$. Given the commonly used assumption of quasi-neutrality in a plasma, the electron number density $n_e = \sum_{i=\text{ions}} n_i$. Moreover, we assume the electron pressure $p_e = \sum_{i=\text{ions}} p_i$ and ignore the heat conduction.

The source terms $\frac{\delta \rho_s}{\delta t}$, $\frac{\delta M_s}{\delta t}$, and $\frac{\delta E_s}{\delta t}$ represent the variations due to particle collisions and chemical reactions among all the species for mass, momentum, and energy, respectively (Li et al. 2020).

The electric field E is defined as $E = -\frac{\nabla p_e}{e n_e} - u_e \times B$. Introducing the charge-averaged ion velocity $u_+ = \frac{1}{e n_e}\sum_s n_s q_s u_s$ and electron velocity $u_e = u_+ - \frac{J}{e n_e}$, the magnetic induction equation can be written as

$$\frac{\partial B}{\partial t} - \nabla \times \left(u_+ \times B - \frac{J \times B}{e n_e} + \frac{\nabla p_e}{e n_e} \right) = 0 \tag{2}$$

where $J = \frac{1}{\mu_0}\nabla \times B$.

The photoionization rates were calculated according to a more rigorous method proposed by Singh & Prasad (1983), which can reproduce the M2 layer of the Martian ionosphere more precisely. Thus, the well-developed 3D multifluid MHD model is capable of generating the Martian ionosphere self-consistently by taking account of particle collisions and chemical reactions including photoionization, charge exchange, and dissociative recombination between individual ion species. The corresponding chemical reactions and rates were adopted from Ma et al. (2004) and Schunk & Nagy (2009).

The Chapman function (Huestis 2001), proved to describe more precisely the M2 layer of the Martian ionosphere (Withers 2009), was used in our model to obtain the optical depth effect in calculating photoionization rates of the neutrals instead of the cosine function of the solar zenith angle that would make the solar flux zero on the nightside. This improvement is able to make our results more precise and reasonable.

The Mars-centered Solar Orbital (MSO) reference frame was adopted in our simulations, where the x-axis points from Mars toward the Sun, the z-axis is perpendicular to the x-axis and positive toward the north celestial pole, and the y-axis completes the right-handed coordinate system. The computational domain

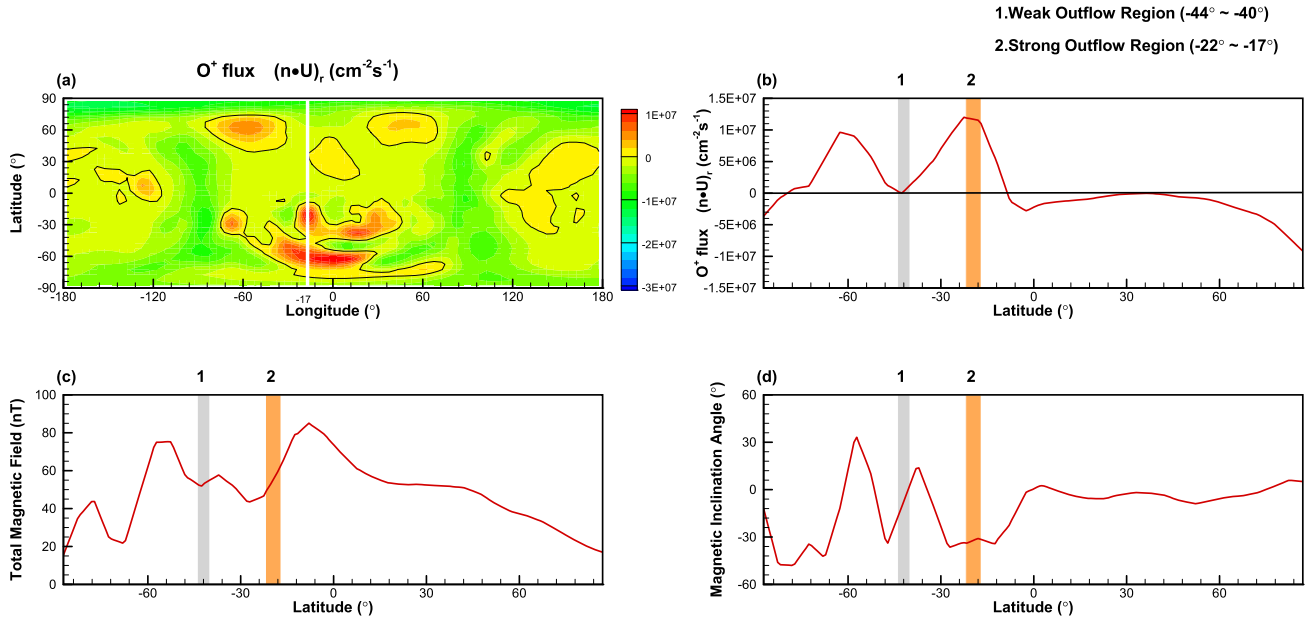

Figure 1. (a) Longitude–latitude map of O^+ flux at 425 km. The variation of O^+ flux (b), total magnetic field strength (c), and inclination angle (d) with latitude at longitude $-17°$ and an altitude of 425 km. The black contour line denotes that the value of flux at this altitude is zero.

was defined as $-24R_M \leqslant X \leqslant 8R_M$, $-16R_M \leqslant Y$, and $Z \leqslant 16R_M$ where R_M is the radius of Mars ($R_M \approx 3396$ km), with the lowest boundary of 100 km above the Martian surface, where the ion densities were taken as the photochemical equilibrium values. An adapted grid used in our simulation consisted of 56 blocks and $100 \times 120 \times 80 = 960{,}000$ computational cells with the finest cell of size 10 km at the lowest inner boundary where the velocity and the density of H^+ were set to be zero and 0.3 of the solar wind densities separately (Dong et al. 2015b). We used the 1D neutral density profile developed by Bougher et al. (2000) as an initial input in order to facilitate the comparison between Martian northern and southern hemispheres. According to the typical solar wind parameters upstream of Mars (Liu et al. 2021), the solar wind density and velocity were chosen to be 4 cm^{-3} and 500 km s^{-1}, respectively. The IMF was assumed to be a Parker spiral with an orientation of 56° and a magnitude of 3 nT in the x–y plane, that is $(B_x, B_y, B_z) = (-1.6, 2.5, 0)$ nT in the MSO coordinate system. The subsolar point is 0° longitude at the equator. A 90° spherical harmonics expansion model proposed by Cain et al. (2003) was adopted for the Martian crustal magnetic field as a reference magnetic field with the strongest field located at about −53° latitude.

3. Simulation Results

In order to study the impact of magnetic inclination angle from a local perspective, we plotted a snapshot of the O^+ ion flux distribution at an altitude of 425 km in Figure 1(a) by transforming from MSO to longitude–latitude–altitude coordinates. The magnetic inclination angle is defined as the angle between the magnetic field lines and the local longitude–latitude plane. Thus, horizontal/vertical magnetic field lines refer to the magnetic field direction parallel/orthogonal to the longitude–latitude plane. In Figures 1(b)–(d), the O^+ ion flux, total magnetic field, and magnetic inclination angle at a longitude of −17° of Figure 1(a) (white line) are plotted, where positive O^+ flux means outward flow while negative flux indicates inward backflow. It can be seen from Figure 1(b) that there are two regions of strong escape flux around latitudes of −60° and −20°, and a region of weak escape flux between them located around latitude −40°. In order to compare the physical features for the different strengths of escape flux, here we define the weak outflow region in latitude from −44° to −40° with a small flux, and the strong outflow region from −22° to −17° with a high flux (labeled 1 and 2 in Figures 1(b), (c), and (d), respectively). It can be seen from Figure 1(c) that the total magnetic fields in the two regions are almost same and about 55 nT. Figure 1(d) demonstrates the variation of magnetic inclination angle, which is defined as the angle between the magnetic field direction and the local horizontal plane. It can be seen from Figure 1(d) that the magnetic inclination angle is about 5° in the weak outflow region and −30° in the strong flux region, which indicates that the magnetic field direction tends toward a less horizontal orientation in the strong outflow region than in the weak one. On the other hand, the total magnetic field strength is almost same in the two regions. Therefore, the outward transport channel due to vertical magnetic field is a more significant factor for ionospheric upwelling to higher altitudes than the strength of magnetic field.

According to the first and second terms on the right-hand side of Equation (1b) in our multifluid MHD model, the electromagnetic (EM) forces acting on the O^+ ion can be expressed as follows:

$$F_{\mathrm{EM}\,O^+} = n_s q_s (u_s \times B + E). \tag{3}$$

Defining $E = -u_+ \times B + \frac{J \times B}{e n_e} - \frac{\nabla p_e}{e n_e}$, the expression for the EM forces can become

$$F_{\mathrm{EM}\,O^+} = n_s q_s (u_s - u_+) \times B + \frac{n_s q_s}{n_e e} J \times B - \frac{n_s q_s}{n_e e} \nabla p_e. \tag{4}$$

The three terms on the right-hand side of Equation (4) correspond to motional electric force, Hall electric force, and electron pressure gradient force. It is important to note that the magnetic field is moving with the charge-averaged ion velocity (u_+) and the motional electric force only acts when the ions are

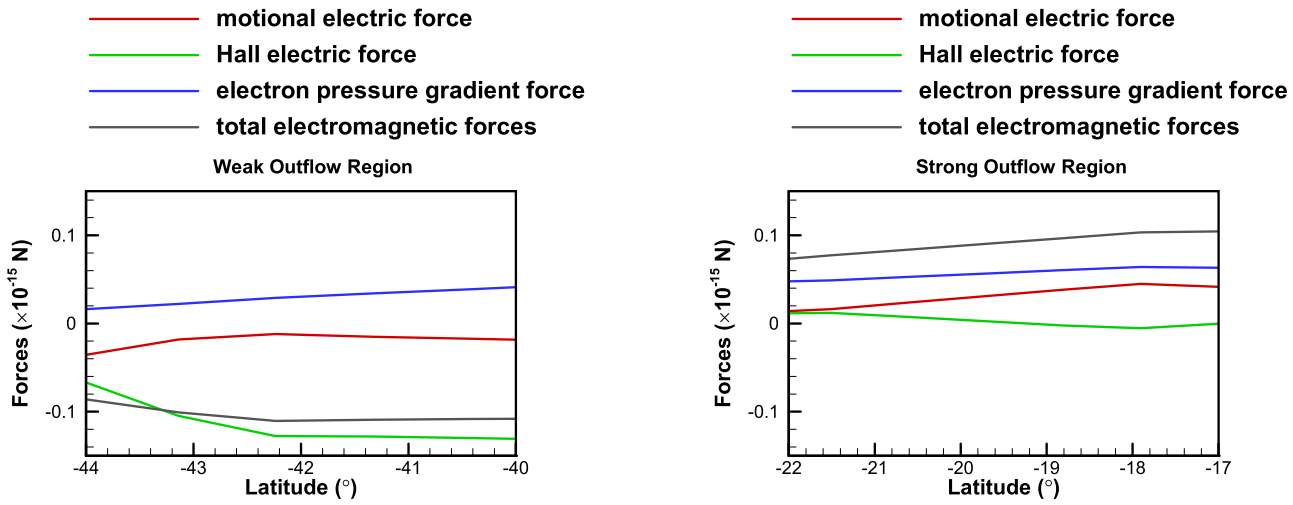

Figure 2. The variation of motional electric force (red line), Hall electric force (green line), electron pressure gradient force (blue line), and total electromagnetic forces (black line) with latitude at longitude −17° and an altitude of 425 km in weak (top) and strong (bottom) outflow regions.

moving across the magnetic field, so the motional electric force on the O^+ ion depends on its velocity relative to u_+ (Ma et al. 2019).

In order to determine the dominant forces driving outward flux, Figure 2 depicts the three force terms in Equation (4) in the two regions. In the weak outflow region, it can be seen that the total EM force is mainly provided by the Hall electric force and it has the opposite direction to the outward O^+ velocity, which means the plasma flow in this region is decelerated by the Hall electric force. Hence the horizontal magnetic field lines suppress O^+ ion escape in the weak flux region. In the strong outflow region, the total EM force is mainly provided by the electron pressure gradient force and motional electric force, and it has the same direction as the outward O^+ velocity, which means the plasma flow in this region is accelerated. Since magnetic field lines with high absolute inclination angle are dominant in the region, they play an important role in enhancing O^+ ion escape. Therefore, it can be concluded that ions tend to get trapped at the local horizontal magnetic equator by the horizontal magnetic field lines due to the Hall electric force, and they diffuse upward along magnetic field lines with high absolute inclination angle to higher altitudes as a result of the electron pressure gradient force and motional electric force.

In order to study the impact of magnetic inclination angle on ion escape from a global perspective, we plotted several snapshots of distributions of O^+ density and flux at altitudes between 275 km and 575 km as shown in Figure 3. It can be seen that at the lowest altitude of 275 km, there is no apparent discrepancy in the O^+ ion density distribution between the northern and southern hemispheres. However, it exhibits different features at higher altitudes of 325 km to 575 km. From Figure 3 (top), the O^+ density is approximately an order of magnitude greater in the southern hemisphere than in the northern hemisphere, especially in the region with larger magnitude and gradient of the crustal magnetic field. Since we used the 1D spherical profiles of neutral components as initial inputs in the simulation model, the initial densities at the corresponding locations in both hemispheres are the same. These results reveal that the Martian crustal magnetic field has an upwelling effect on the ion distribution in the ionosphere, which increases the O^+ ion density over the crustal field area.

However, the variation of O^+ flux distributions with altitude from 275 km to 575 km is more complicated, as shown in Figure 3 (bottom). It is obvious that the ion escape flux is high in the region with strong crustal magnetic fields in the southern hemisphere. In order to understand the impact of the crustal magnetic field, a numerical case in the absence of the crustal field was calculated. Comparing with the case used in this paper, the morphology of ion fluxes in the southern hemisphere derived from the simulation without the crustal field is more similar to that in the northern hemisphere in Figure 3 where the impact of the anomaly can be ignored. In other words, the presence of a crustal magnetic field enhances the ion escape flux in the southern hemisphere. Therefore, there are reasons to believe that it is the interaction between the Martian crustal magnetic field and the IMF that provides a transport channel for driving ion escape from Mars.

Therefore, the conclusion can be drawn that the density and flux of O^+ ions in the southern hemisphere with strong crustal fields are larger than those in the corresponding northern hemisphere. It can be explained that O^+ ions move to higher altitudes along magnetic field lines with high absolute inclination angle, resulting in a concentration of O^+ ions and an enhancement of O^+ escape flux in the southern hemisphere. Our results are consistent with Matta et al. (2015), who, by using a 2D ionospheric model, suggested that the ionosphere is more inflated over the vertical field region than in other regions.

The distributions of total magnetic field strength and inclination angle at 425 km are plotted in Figure 4, along with contour lines denoting the magnitude of the total magnetic field. A strong positive correlation is indicated between the local magnetic field strength and magnetic inclination angle on the dayside. Therefore, it can be concluded that the strong crustal field regions in the southern hemisphere are mainly occupied by magnetic field lines with high absolute inclination angle, whereas horizontal field lines are dominant in the northern hemisphere, which is consistent with the statistical results from MAVEN Magnetometer level 2 data published by Wu et al. (2019). In addition, the magnetic field lines with high absolute inclination angle in the southern hemisphere have both inward and outward directions, between which horizontal field lines exist; this can be described as a “mini-magnetosphere” as

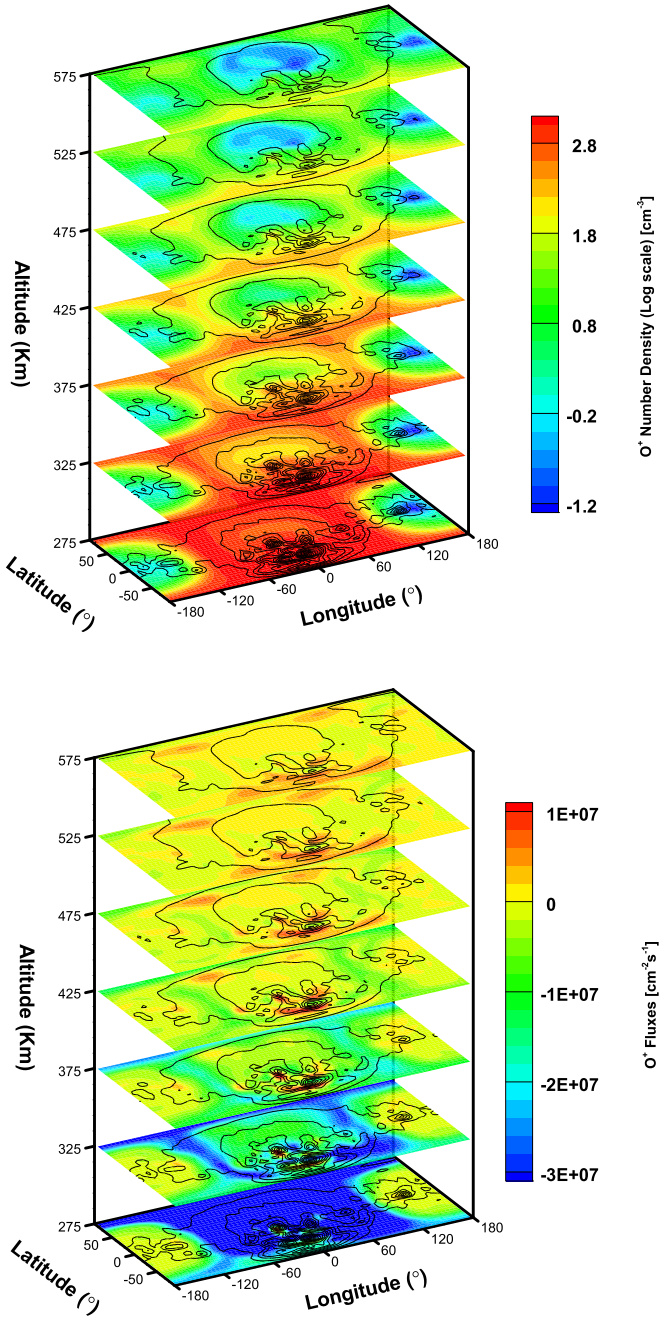

Figure 3. Maps of O^+ ion density (top) and flux (bottom) as a function of longitude and latitude for several slices of altitude (275–575 km). The black contour line denotes the total magnetic field at each altitude.

studied from observations and numerical simulations (Lundin et al. 2011; Egan et al. 2019). Moreover, comparison between the distributions of absolute inclination angle and O^+ ion flux from Figures 3 and 4 indicates that O^+ ion fluxes are high in the region with high absolute magnetic inclination angle in the Martian southern hemisphere, whereas the fluxes are weak in the northern hemisphere with horizontal field lines. Therefore, the Martian southern hemisphere possesses more magnetic field lines with high absolute inclination angle than the northern one. The more vertical the magnetic field lines are, the more favorable the upward transport of O^+ ions is. Similar results were found by Weber et al. (2021), who used the MAVEN spacecraft data to statistically analyze how crustal magnetic fields influence ion escape and suggested that many of the energized ions should have a direct path along open field lines by which they can escape.

In order to evaluate the global influence of the Martian magnetic field on the O^+ escape, Table 1 provides the total O^+ escape rate from 275 km to 1000 km in the southern and northern hemispheres separately. It can be seen that the O^+ escape rate is much higher in the southern hemisphere than in the northern one, even twice as large at high altitude. Based on the analysis in this paper, the explanation is that the southern hemisphere possesses more magnetic field lines with high absolute inclination angle to transport O^+ ions upwards. It is worth noticing that the inward O^+ fluxes due to backflow are prevalent at lower altitudes in both hemispheres, which is consistent with maps of ion radial velocity in the northern/southern quadrants provided by Dubinin et al. (2020), who suggested that the direction of ion velocity is inward at altitudes below around 400 km. Moreover, the backflow rate is smaller in the southern hemisphere than in the northern one, which can be explained by the flux distributions in Figure 3 where the southern hemisphere has a strong outflow area over the Martian crustal field at lower altitudes.

4. Discussions and Conclusion

A global multifluid MHD simulation was conducted to evaluate the impact and mechanism of magnetic inclination angle on O^+ escape during the interaction between the solar wind and the Martian atmosphere. The well-developed MHD model used in this study can self-consistently reproduce the Martian ionosphere by considering the production and loss of the main ionospheric ion species associated with physical collisions and chemical reactions among these species. Cain's crustal field model was adopted with the strongest field aligned at about $-53°$ latitude in our time-independent simulation.

There is no doubt that the presence of crustal field has a significant impact on the interaction between the solar wind and the Martian ionosphere. One of the most interesting subjects is the influence of crustal anomaly on ion escape from the Martian atmosphere, which may contribute to the change in its long-term climate. However, the answer to this question is complex. Previous research has offered three different conclusions on this matter: the protection effect of crustal fields manifesting when relevant solar zenith angle is small, enhancement of ion escape due to the creation of an additional outflow channel, and the varying influence of the magnetic shield depending on the historical strength of the magnetic field.

In this study, the importance of a transport channel was accounted for by considering chemical interactions and typical solar wind input conditions. The Martian magnetic field lines are in a state of disorder during the interaction between the Martian crustal field and interplanetary magnetic field. However, at low altitudes of 275–1000 km above the Martian surface, the magnetic field directions can be categorized into two types, horizontal and vertical, which indicates that the magnetic inclination angle has a significant influence on escape of ions.

From a local perspective, ions are likely to get trapped at the local horizontal magnetic equator due to the Hall electric force, but to diffuse upward along the magnetic field lines with high absolute magnetic inclination angle, as a result of the electron pressure gradient force and motional electric force. From a global perspective, there are more magnetic field lines with

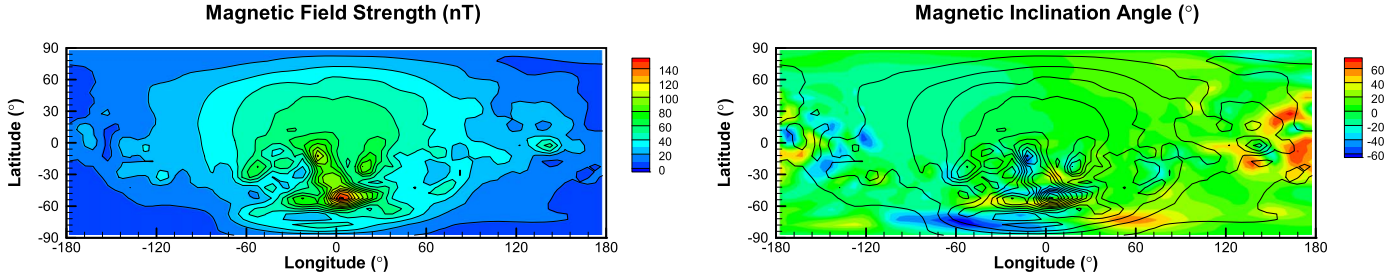

Figure 4. Longitude–latitude map of total magnetic field strength (top) and inclination angle (bottom) at 425 km. Black contour lines denote the total magnetic field at this altitude.

Table 1
O^+ Ion Escape Rates (s^{-1}) for the Whole Planet and the Two Separate Hemispheres at Several Altitudes from 275 km to 1000 km

Altitude (km)	Southern Hemisphere ($\times 10^{22}$ s^{-1})	Northern Hemisphere ($\times 10^{22}$ s^{-1})	Total Escape Rate ($\times 10^{22}$ s^{-1})
275	−10.5	−13.1	−23.6
375	−5.86	−6.38	−12.24
475	0.11	−0.76	−0.65
575	2.05	0.71	2.76
800	4.66	2.33	6.99
1000	6.34	3.53	9.87

high absolute inclination angle clustered in the southern hemisphere, while horizontal field lines are dominant in the northern hemisphere during the interaction between the Martian crustal field and interplanetary magnetic field. Therefore, the southern ionosphere is more extended than the northern counterpart. Moreover, O^+ ion escape rates are larger in the Martian southern hemisphere than in the northern one at altitudes from 275 km to 1000 km. Since the strength and influence of the Martian crustal field decline quickly above 1000 km (Ramstad et al. 2016), O^+ ions can escape due to some other escape mechanisms such as pickup (Dong et al. 2015a) and Hall acceleration in the plasma sheet (Dubinin et al. 2017a).

The magnetic field in the Martian southern hemisphere has both inward and outward directions as well as being horizontal (see Figure 4), which is similar to the magnetic topology of a so-called mini-magnetosphere. It has been proven that the mini-magnetosphere can protect ions from escape from the Martian ionosphere (Lundin et al. 2011; Egan et al. 2019), which can result from the suppression of ion motion by horizontal magnetic field lines. On the other hand, Fan et al. (2019) have shown an area characterized by lower fluxes of high energy ($E \geqslant 30$ eV) O^+ ions above the region of crustal magnetic field. There are reasons to believe that it is caused by the protective effect due to the horizontal magnetic field lines.

The necessary requirements for ion escape from the Martian atmosphere/ionosphere include ion supply, solar wind energy transfer, and a transport channel (Ramstad & Barabash 2021), each of which can be a bottleneck to the escape process. In the absence of an escape channel controlled by the vertical magnetic field lines, ions with the necessary energy for escape still can be trapped by the closed magnetic field topology or precipitate due to collisional processes. In spite of the considerable transport channel controlled by the vertical magnetic field lines, the effects of ion supply and solar wind energy transfer on ion escape cannot be neglected. The supply of ions can be affected by ionization efficiency (e.g., Dubinin et al. 2017b; Cui et al. 2018), whereas the energy input may control by the interplanetary magnetic field direction (e.g., Weber et al. 2020; Sakai et al. 2021) and solar wind conditions (e.g., Nilsson et al. 2011; Ramstad et al. 2015; Ramstad & Barabash 2021). However, this study only considers the typical solar wind conditions as well as the strength and direction of the interplanetary magnetic field. Weber et al. (2019) suggest that high solar wind pressure decreases the presence of closed topology across Mars and that its ionosphere becomes more exposed to the solar wind energy input. The direction of the interplanetary magnetic field determines the area of open or closed magnetic field topology to the solar wind. Moreover, the rotation of the crustal magnetic field with Mars also changes the distribution of Martian magnetic field lines, which has an important effect on ion escape. These subjects are interesting and important, and will be studied in our future work.

This work was supported by the B-type Strategic Priority Program of the Chinese Academy of Sciences (grant No. XDB41000000) and the pre-research projects on Civil Aerospace Technologies No. D020103 and D020105 funded by China's National Space Administration (CNSA), and the National Natural Science Foundation of China (NSFC) under grants No. 42074214, 41922031, and 41821003. J.A.W. was supported by STFC Consolidated Grant ST/R000816/1.

ORCID iDs

Shibang Li https://orcid.org/0000-0001-9175-0007
Christian Mazelle https://orcid.org/0000-0001-5332-9561
Jun Cui https://orcid.org/0000-0002-4721-8184
Zhaojin Rong https://orcid.org/0000-0003-4609-4519

References

Acuña, M. H., Connerney, J., Wasilewski, P., et al. 2001, JGR, 106, 23403
Airapetian, V. S., Glocer, A., Khazanov, G. V., et al. 2017, ApJL, 836, L3
Benna, M., Mahaffy, P. R., Grebowsky, J. M., et al. 2015, GeoRL, 42, 8958
Bougher, S. W., Engel, S., Roble, R. G., et al. 2000, JGR, 105, 17669
Bougher, S. W., Pawlowski, D., Bell, J. M., et al. 2015, JGRE, 120, 311
Brain, D. A., Baker, A. H., Briggs, J., et al. 2010, GeoRL, 37, L14108
Cain, J. C., Ferguson, B. B., & Mozzoni, D. 2003, JGRE, 108, 5008
Carr, M. H. 1986, Icar, 68, 187

Carr, M. H. 2007, The Surface of Mars (London: Cambridge Univ. Press)
Chicarro, A., Martin, P., & Trautner, R. 2004, in ESA Special Publication 1240, Mars Express: The Scientific Payload, ed. A. Wilson (Noordwijk: ESA), 3
Collinson, G., Mitchell, D., Glocer, A., et al. 2015, GeoRL, 42, 9128
Connerney, J. E. P., Acua, M. H., Wasilewski, P. J., et al. 1999, Sci, 284, 794
Cui, J., Cao, Y. T., Wu, X. S., et al. 2019, ApJL, 876, L12
Cui, J., Wu, X. S., Xu, S. S., et al. 2018, ApJ, 857, L18
Dong, C., Bougher, S. W., Ma, Y., et al. 2015b, JGRA, 120, 7857
Dong, C., Lee, Y., Ma, Y., et al. 2018, ApJL, 859, L14
Dong, C., Lingam, M., Ma, Y., et al. 2017, ApJL, 837, L26
Dong, Y., Fang, X., Brain, D. A., et al. 2015a, GeoRL, 42, 8942
Dubinin, E., Fraenz, M., Pätzold, M., et al. 2017a, JGRA, 122, 11285
Dubinin, E., Fraenz, M., Pätzold, M., et al. 2017b, JGRA, 122, 7142
Dubinin, E., Fraenz, M., Pätzold, M., et al. 2020, JGRA, 125, e2020JA028010
Egan, H., Jarvinen, R., Ma, Y., et al. 2019, MNRAS, 488, 2108
Fan, K., Fraenz, M., Wei, Y., et al. 2019, GeoRL, 46, 11764
Fränz, M., Dubinin, E., Andrews, D., et al. 2015, P&SS, 119, 92
Halekas, J. S., Brain, D. A., Lillis, R. J., et al. 2006, GeoRL, 33, L13101
Harnett, E. M. 2009, JGRA, 114, A01208
Huestis, D. L. 2001, JQSRT, 69, 709
Jakosky, B. M., Brain, D., Chaffin, M., et al. 2018, Icar, 315, 146
Jakosky, B. M., & Phillips, R. J. 2001, Natur, 412, 237
Jakosky, B. M., & Russell, C. T. 2015, SSRv, 195, 1
Jakosky, B. M., Slipski, M., Benna, M., et al. 2017, Sci, 355, 1408
Johnson, R. E., & Leblanc, F. 2001, in Physics of Space: Growth Points and Problems, ed. N. Meyer-Vernet et al. (Dordrecht: Springer), 259
Langlais, B., Purucker, M. E., & Mandea, M. 2004, JGRE, 109, E02008
Li, S. B., Lu, H. Y., Cui, J., et al. 2020, E&PP, 4, 23
Lillis, R. J., Brain, D. A., Bougher, S. W., et al. 2015, SSRv, 195, 357
Liu, D., Rong, Z. J., Gao, J. W., et al. 2021, ApJ, 911, 113
Lundin, R., Barabash, S., Yamauchi, M., et al. 2011, GeoRL, 38, L02102
Ma, Y., Dong, C., Toth, G., et al. 2019, JGRA, 124, 9040
Ma, Y., Fang, X., Russell, C. T., et al. 2014, GeoRL, 41, 6563
Ma, Y., Nagy, A. F., Sokolov, I. V., et al. 2004, JGRA, 109, A07211
Mahaffy, P. R., Benna, M., Elrod, M., et al. 2015, GeoRL, 42, 8951
Matta, M., Mendillo, M., Withers, P., et al. 2015, JGRA, 120, 766
Nagy, A. F., Winterhalter, D., Sauer, K., et al. 2004, SSRv, 111, 33
Najib, D., Nagy, A. F., Tóth, G., et al. 2011, JGRA, 116, A05204
Nilsson, H., Edberg, N., Stenberg, G., et al. 2011, Icar, 215, 475
Ramstad, R., & Barabash, S. 2021, SSRv, 217, 36
Ramstad, R., Barabash, S., Futaana, Y., et al. 2015, JGRE, 120, 1298
Ramstad, R., Barabash, S., Futaana, Y., et al. 2016, GeoRL, 43, 10574
Sakai, S., Seki, K., Terada, N., et al. 2018, GeoRL, 45, 9336
Sakai, S., Seki, K., Terada, N., et al. 2021, JGRA, 126, e2020JA028485
Schunk, R. W., & Nagy, A. F. 2009, Ionospheres (2nd ed.; New York: Cambridge Univ. Press)
Seager, S. 2013, Sci, 340, 577
Shizgal, B. D., & Arkos, G. G. 1996, RvGeo, 34, 483
Singh, R. N., & Prasad, R. J. 1983, JApA, 4, 261
Wan, W. X., Wang, C., Li, C. L., et al. 2020, NatAs, 4, 721
Weber, T., Brain, D., Mitchell, D., et al. 2019, GeoRL, 46, 2347
Weber, T., Brain, D., Xu, S., et al. 2020, GeoRL, 47, e2020GL087757
Weber, T., Brain, D., Xu, S., et al. 2021, JGRA, 126, e2021JA029234
Withers, P. 2009, AdSpR, 44, 277
Wu, X. S., Cui, J., Xu, S. S., et al. 2019, JGRE, 124, 734
Xu, S., Mitchell, D., Liemohn, M. W., et al. 2016, GeoRL, 43, 8876